ScieRxiv

NOT PEER-REVIEWED

Article

Polymer-binder-free $LiFePO_4$ cathodes with Li^+-containing organic ionic plastic crystals for high-energy and high-power lithium-ion batteries

Daniela M. Josepetti[1,#], Maria Forsyth[1,2], Patrick C. Howlett[1,2], Hiroyuki Ueda[1,2,*]

[1]Institute for Frontier Materials (IFM), Deakin University, 221 Burwood Highway, Burwood, Victoria 3125, Australia.
[2]Battery Research and Innovation Hub, Deakin University, 5/154 Highbury Road, Burwood, Victoria 3125, Australia.

***Correspondence to:** Dr. Hiroyuki Ueda, Institute for Frontier Materials (IFM), Deakin University, 221 Burwood Highway, Burwood, Victoria, Australia. E-mail: h.ueda@deakin.edu.au.

Present Address: #D.M.J.: Pôle Chimie Balard Recherche, 1919 route de Mende, 34293 Montpellier, France.

Received: 20 August 2024 | Approved: 22 August 2024 | Online: 27 August 2024

Abstract

Lithium-ion batteries are a promising technology to promote the phase-out of fossil fuel vehicles. Increasing efforts are focused on improving their energy density and safety by replacing current materials with more efficient and safer alternatives. In this context, binary composites of organic ionic plastic crystals (OIPCs) and lithium salts show promise due to their impressive mechanical properties and ionic conductivity. Taking advantage of this, the present paper substitutes the commercial non-electrochemically active binder with an OIPC component, *N*-ethyl-*N*-methylpyrrolidinium bis(fluorosulfonyl)imide ([C_2mpyr][FSI]), in combination with LiFSI. Slurry-formulation experiments revealed that varying the new binder's composition allows the production of diverse $LiFePO_4$ (LFP) cathodes *via* the conventional fabrication process. High concentrations of OIPC−lithium salt in the compositions yielded electrodes with high energy densities (nominal areal capacities of up to 3.74 mAh/cm²), exhibiting satisfactory cycling performance with proper lithiation/delithiation reactions of LFP. A reduced Li^+ concentration of OIPC−lithium salt enabled LFP cathodes to perform effectively under fast cycling conditions at a C-rate as high as 2C. Preliminary battery tests with a limited Li^+ source demonstrated the feasibility of full-cell operation without using the lithium−metal anode. This work paves the way for developing safe, rechargeable batteries using OIPC-based ion-conductive binders for a wide range of applications.

Keywords: Polymer-binder-free cathodes, Ion-conductive binders, Organic ionic plastic crystals, Ionic liquids, Lithium−metal batteries, Rechargeable batteries, Lithium iron(II) phosphate, Composite cathodes

1. INTRODUCTION

The development of rechargeable batteries with high energy density can address the increasing demand for low-emission greenhouse gas vehicles and mobile devices with extended operational duration (while unplugged from electricity)[1]. In fact, lithium-ion batteries (LIBs) are already responsible for outstanding

DOI: 10.20517/scierxiv202408.01.v1 https://www.scierxiv.com/

progress in portable electronics and electric cars in terms of energy autonomy and durability[2]. This battery technology, when compared with other commercial rechargeable batteries, exhibits a relatively high energy density, low self-discharge, and low memory effect[3-6]. On the other hand, the current LIBs have approached their theoretical capacities sufficiently[7,8], which limits the continuous improvement of their energy density unless their cell chemistries are changed, and other issues such as environmental and safety concerns hinder their prevalent use[9].

In that sense, the evaluation of new materials for advanced LIBs is appealing because it could offer a solution to some of these drawbacks. One strategy to increase energy density is to reduce electrochemically non-functional materials in the electrode formulation, such as the binder (that is generally a non-electron and non-ion conductive polymer). The most employed commercial binder is poly(vinylidene fluoride) (PVDF), primarily due to its high electrochemical stability[10]. However, PVDF in typical LIB electrodes is added solely to hold the electrode components (*i.e.*, active material, conductive material, and current collector) together and its electrical conductivity is almost negligible (*i.e.*, $<10^{-10}$ S cm^{-1} at room temperature[11]). Therefore, reducing the weight ratio of a polymer binder in an electrode would provide the electrode with a higher electrical conductivity[12-14], which often sacrifices the mechanical strength of the electrode[12,13,15]. Alternatively, replacing the non-conductive binder with an ion-conductive one is expected to improve the electrochemical performance of electrodes[16-19], while maintaining the necessary mechanical stability of the electrodes for pressing, cell assembly, and battery operation. In addition, this strategy could avoid excess electrolyte solution in the pores of electrodes thereby reducing the required mass of the electrolyte solution. Both consequences lead to an increase in the energy density of the cell. Although such ion-conductive binders have been actively studied for solid-state batteries (as solid polymer electrolytes)[20-22], they have also been demonstrated as useful materials in advanced LIBs using liquid electrolyte solutions[17-19]. Hence, further material exploitation in this direction is worth pursuing to overcome the performance limitations stemming from the conventional non-conductive binders.

One category of ion-conductive materials that shows promise is organic ionic plastic crystals (OIPCs), which are structural analogs of ionic liquids (ILs) but are solids at room temperature[23,24]. OIPCs are typically composed of organic cations that are paired with inorganic anions[25]. Lattice defects and various motions (*e.g.*, rotational, translational, or conformational) of cations and/or anions can cause ion conduction through the 3D lattice of OIPCs, which are beneficial for ions (*e.g.*, Li^+) to move through the media[26]. Additionally, short-range ion motion under stress and the presence of slip-plane defects contribute to the plastic properties of OIPCs[27]. Since the discovery of the improvement of ionic conductivity after the addition of lithium salt to OIPCs[28], they have attracted researcher's attention as novel electrolytes for advanced rechargeable batteries[29-32]. Even a small amount of metal-salt addition can result in a significant improvement in ion transport (including added metal ions such as Li^+)[33,34]. The formation of a liquid phase in this binary mixture of an OIPC and a metal salt also contributes to the enhanced ion conduction of the medium[28,35]. In some binary mixtures, an increase in the metal-salt concentration increases the volume fraction of a liquid phase in the OIPC−metal-salt composite. Interestingly, these binary mixtures often maintain a solid phase until a certain level of metal-ion inclusion[27], after which an ionic liquid is formed.

Because of such promising ion-conduction properties of OIPC electrolytes, they have been studied as solid-electrolyte membranes for solid-state batteries[29,32,36]. In recent years, they have also been used as additional integrated ion-conduction pathways in solid-state electrodes[23,37-43]. These studies have demonstrated the huge potential of OIPC electrolytes as functional ion-conductive materials for advanced rechargeable batteries. As OIPC electrolytes are non-volatile and non-flammable materials like ILs, their use in rechargeable batteries is advantageous for addressing safety issues[44]. This could potentially offer the same preferred features as ILs in device operation; for instance, highly Li^+-concentrated ILs have shown promising results in terms of improved cycling performance[45,46] and even dendrite suppression[45]. However, to the best of our knowledge, past studies on OIPC-containing electrodes still required binders to keep the electrodes intact and additional functionality of OIPC

electrolytes as binders in electrodes has yet to be explored in detail. The use of OIPC electrolytes as binders seems possible because the mechanical properties of OIPCs depend on their constituent ions and some pure OIPCs are reportedly sticky, including the ones with bis(fluorosulfonyl)imide ($[FSI]^-$) anions[47,48].

In this context, our present study took advantage of the ion-conduction and mechanical properties of Li^+-containing OIPCs comprising *N*-ethyl-*N*-methylpyrrolidinium ($[C_2mpyr]^+$) cations and $[FSI]^-$ anions (hereafter referred to as $Li_x[C_2mpyr]_{1-x}[FSI]$), and substituted the commercial polymer binder with them to offer novel polymer-binder-free electrodes for advanced lithium-ion batteries. The addition of lithium salt to this OIPC was carried out to make the composites Li^+ conductors as well as provide a Li^+ source for electrochemical reactions at both electrodes. The lithium salts with identical anions as the OIPC are typically selected for simplicity, where the binary mixture has three constituents: OIPC cations, OIPC anions, and Li^+ ions; in this case, Li^+ ions are regarded as a replacement for OIPC cations in the 3D lattice[26]. $LiFePO_4$ (LFP) was chosen as a cathode active material because of its excellent cyclability[49] and safety (*e.g.*, comparatively low sensitivity against an internal short circuit)[50], and we investigated if the polymer-binder-free approach can provide the resulting LFP composite cathodes with a higher electrode loading than the counterpart with a PVDF binder. Specifically, we explored the effect of electrode formulations on the electrode-fabrication process, whose variables include (*i*) Li^+ concentrations in $Li_x[C_2mpyr]_{1-x}[FSI]$ (*i.e.*, 1, 10, and 50 mol%) and (*ii*) weight ratios of new ion-conductive binder ($Li_x[C_2mpyr]_{1-x}[FSI]$) in the electrode (*i.e.*, 15, 30, and 50 wt%). Some LFP−$Li_x[C_2mpyr]_{1-x}[FSI]$ composite cathodes that were promising for high-energy-density or high-power-density batteries were employed for cell evaluation in a lithium-metal-battery (LMB) configuration. Finally, the polymer-binder-free LFP−$Li_x[C_2mpyr]_{1-x}[FSI]$ was placed in the condition where an excessive Li^+ source (*i.e.*, Li metal anode) is not available (*i.e.*, paired with graphite−$Li_{0.10}[C_2mpyr]_{0.90}[FSI]$ anode) and preliminary demonstration of its full-cell operation progresses the realization of safe OIPC-based rechargeable batteries based on intercalation chemistry.

2. METHODS

2.1. Cathode formulation

2.1.1. Polymer-binder-containing cathode formulation

For the preparation of a cathode with a polymer binder, the active material was LFP (Aleees, M121), the electron-conductive additive was carbon black (Imerys Graphite & Carbon, C-nergy Super C65), the binder was PVDF (Solvay, Solef 5130), and the solvent was *N*-methyl-2-pyrrolidone (NMP, Sigma-Aldrich, 99%). First, the PVDF binder was dissolved in NMP to formulate a 10 wt% solution, which facilitates homogenization of an electrode slurry later. In atmospheric conditions, 84 wt% of LFP, 10 wt% of carbon black, and 6 wt% of PVDF were mixed with NMP using a spatula. After that, all the compounds were mixed with three ϕ5 mm zirconia balls using a planetary ball mill (Retsch, PM 100) for 48 minutes (*i.e.*, 8 cycles of five-minute mixing and one-minute rest, where the mixing direction was reversed every cycle) at 300 rpm. The solvent was added until the viscosity of the slurry became coatable (the final solid-content ratio of the slurry was 35%). In a laboratory doctor blade film coater (Xiamen Tmax Battery Equipments Limited, TMAX-TMH), the mixed slurry was coated on aluminium (15 µm thickness) or carbon-coated aluminium (18 µm total thickness with 1.5 µm carbon thickness per side) sheets with three different wet gaps: 100, 500, and 1,000 µm. The coated sheets were dried at 50 °C for >12 h in an ambient condition and transferred to an Ar-filled glove box (with O_2 < 10 ppm and H_2O < 0.1 ppm) for storage. Test electrodes for coin-cell experiments were made by punching the coated sheets into ϕ14 mm disks and pressing using a pellet die (ϕ16 mm) at room temperature under 0.5 MPa of pressure (which was done outside the glove box). The electrode disks were also dried in a vacuum at 50 °C for >12 h before cell assembly in the glove box.

2.1.2. Polymer-binder-free cathode formulation

The preparation of polymer-binder-free slurry followed a similar procedure for polymer-binder cathodes (Section 2.1.1). The active material, conductive additive, and solvent were the same, but this time, the binder was a binary mixture of [C_2mpyr][FSI] (Boron Molecular, >99%) and LiFSI (Nippon Shokubai, IONEL™ LF-101). The procedure started with drying [C_2mpyr][FSI] in a vacuum at 50 °C for >12 h. Both [C_2mpyr][FSI] and LiFSI were weighed in the glove box. The preparation method of this OIPC-containing slurry is regarded as the "*all-in-one*" method[23,38], where all ingredients are added at once for mixing, but the obvious difference from the previous studies using water-based slurries is that no secondary solvents are needed because both [C_2mpyr][FSI] and LiFSI dissolve in NMP well. In atmospheric conditions, [C_2mpyr][FSI] and LiFSI were mixed with LFP and carbon black in NMP. A homogeneous slurry was obtained by mixing it in the ball mill. Additional NMP was added until the viscosity of the slurry became coatable after mixing by hand using a spatula (the final solid-content ratio was between 35 and 60 wt%). The subsequent steps (*i.e.*, slurry coating, vacuum drying, electrode preservation, electrode punching, and electrode pressing) were also the same as those described in Section 2.1.1. The weight percentages of LFP and carbon black were fixed to 90:10 wt% and their individual weight ratios in the final polymer-binder-free LFP−Li_x[C_2mpyr]$_{1-x}$[FSI] composite electrodes were dependent on the fraction of Li_x[C_2mpyr]$_{1-x}$[FSI]. Table 1 summarizes the electrode formulations of the polymer-binder-free LFP−Li_x[C_2mpyr]$_{1-x}$[FSI] composite cathodes made in this study.

Table 1. Electrode formulations of the polymer-binder-free LFP−Li_x[C_2mpyr]$_{1-x}$[FSI] composite electrodes and polymer-binder containing LFP electrode.

Label	LFP + carbon black : Li_x[C_2mpyr]$_{1-x}$[FSI] [wt%]	[C_2mpyr]$^+$: Li^+ [mol%]	Weight ratio [wt%]				
			LFP (M121)	Carbon black (Super C65)	[C_2mpyr][FSI]	LiFSI (LF-101)	PVDF (Solef 5130)
LFP−15w-Li0.01	85 : 15	99 : 1	77.27	8.61	14.02	0.09	0
LFP−15w-Li0.10	85 : 15	90 : 10	77.38	8.61	13.11	0.90	0
LFP−15w-Li0.50	85 : 15	50 : 50	77.28	8.59	8.64	5.49	0
LFP−30w-Li0.10	70 : 30	90 : 10	62.48	7.51	28.02	1.99	0
LFP−30w-Li0.50	70 : 30	50 : 50	62.48	7.50	18.36	11.66	0
LFP−50w-Li0.01	50 : 50	99 : 1	44.64	5.36	49.68	0.32	0
LFP−50w-Li0.10	50 : 50	90 : 10	44.63	5.36	46.70	3.31	0
LFP−50w-Li0.50	50 : 50	50 : 50	44.61	5.36	30.61	19.42	0
LFP−6w-PVDF (Reference)	100 : 0	N/A	84.04	9.88	0	0	6.08

2.2. Battery tests

2.2.1. Coin cell assembly

Experiments were performed in coin cells using a CR2032 format. For the LMB configuration, both sides of the lithium foil (Ganfeng Lithium, thickness of 50 µm) were brushed before the foil was punched into disks (ϕ16 mm). The electrolyte was an IL with the same constituent ions as the

ion-conductive binder, *i.e.*, $Li_{0.50}[C_2mpyr]_{0.50}[FSI]$. Coin cells were assembled in the glove box and followed the stacking order from the bottom to top: a negative case, 1 mm spacer, anode (either a lithium-metal disk or preconditioned graphite−$Li_{0.10}[C_2mpyr]_{0.90}[FSI]$ anode disk), separator (Celgard 3501 in ϕ19 mm) filled with 100 µL of $Li_{0.50}[C_2mpyr]_{0.50}[FSI]$, testing cathode (*i.e.*, polymer-binder-free LFP−$Li_x[C_2mpyr]_{1-x}[FSI]$ composite), 0.5 mm spacer, spring, and positive case with a gasket.

For experiments in a full-cell setup, a previously studied graphite−$Li_{0.10}[C_2mpyr]_{0.90}[FSI]$ anode comprising 63.0 wt% of graphite, 3.50 wt% of carbon black (Super C65), 3.50 wt% of Na-CMC (Sigma-Aldrich, average molecular weight: 70,000 g/mol), and 30.0 wt% of $Li_{0.10}[C_2mpyr]_{0.90}[FSI]$ was used [23]. This electrode was preconditioned in a solid-state half-cell comprising Li | electrospun PVDF−$Li_{0.10}[C_2mpyr]_{0.90}[FSI]$ solid-electrolyte membrane | graphite−$Li_{0.10}[C_2mpyr]_{0.90}[FSI]$ anode at 0.1C, 50 °C for three cycles [23]. After the formation of SEI on graphite through this procedure, the preconditioned graphite−$Li_{0.10}[C_2mpyr]_{0.90}[FSI]$ anode was taken from the disassembled cell in the glove box and used for full-cell assembly.

2.2.2. Electrochemical tests

The galvanostatic charge and discharge were carried out using the Neware battery cycler at 50 °C. The first step was a 10-hour rest at the open circuit voltage (OCV). After that, the constant-current-constant-voltage (CCCV) mode was applied with a current rate of 0.1C, with 10 minutes of resting time between charging and discharging. The maximum capacities of the cathodes were calculated considering 150 mAh/g as the nominal capacity for the LFP. Then, this nominal value was multiplied by the active material mass present on the cathode, resulting in the considered 1C capacity. The nominal capacity was set based on the discharge capacity of our reference cathode (*i.e.*, LFP−6w-PVDF) in LP30 (*i.e.*, 1 M $LiPF_6$ in ethylene carbonate and dimethyl carbonate with 50 : 50 vol%) as a liquid electrolyte solution, which was sufficiently close to the supplier's capacity value of this LFP on its certificate of analysis (*i.e.*, 154 mAh/g, see Section 3.3.1 for details). The cut-off voltages were 2.5 and 4.2 V. Three preliminary cycling experiments were performed. When these three cycles showed expected behaviors as described in the literature reference for LFP (*i.e.*, low polarization, the plateau at ≈3.4 V, and the discharge capacity of ≈150 mAh/g)[51], the cathode was further charged and discharged for 10 more cycles. The test parameters for this further aging experiment were the same as the first three cycles, but the 1C nominal capacity was updated to the experimental one; *i.e.*, the capacity obtained in the third discharge step was considered as the cell capacity. After a total of 13 cycles, the rate-capability experiments were performed with the sequence: 0.1C (reference value) → 0.2C → 0.5C → 1C → 2C. To evaluate charge and discharge rate capabilities separately, either the charge or discharge rate was changed, and the other rate was kept constant (*i.e.*, 0.1C). After the rate tests, long-term cycling (80 cycles) tests were conducted, which followed the same test parameters as the 10 extra cycles.

2.3. Scanning electron microscopy and energy-dispersive X-ray

Some cathodes were structurally analyzed before cycling *via* scanning electronic microscopy (SEM) using a JSM IT 300 series microscope. Energy dispersive X-ray (EDX) experiments were performed in the same machine by an Oxford X-Max 50 mm^2 EDX detector. The samples for cross-sectional observations were prepared by the procedure described previously[23]. Samples were placed on the stage of an air-sensitive holder in the glove box and transferred to the antechamber of the microscope. This ensures that all the images were unaffected by the ambient conditions (*e.g.*, moisture).

3. RESULTS AND DISCUSSION

3.1. Effect of the $Li_x[C_2mpyr]_{1-x}[FSI]$ content and Li^+ concentration on the nominal areal capacity and electrode density of the composite electrode

The polymer-binder-free slurry was prepared in the "*all-in-one*" method[38], as illustrated in Figure 1a.

This mixing protocol follows the same steps as regular polymer-binder cathode slurries[24] and does not involve any additional manufacturing processes. Here we chose NMP as a solvent because $[FSI]^-$-based OIPCs do not dissolve in water, but future works will explore electrode-preparation methods using more environmentally benign solvents than NMP (*e.g.*, pre-compositing the OIPCs with one of the other electrode ingredients[23]). This choice also allows a more direct comparison with the traditional PVDF coating procedure. The effect of the two different types of proportions was evaluated, which included the quantity of $Li_x[C_2mpyr]_{1-x}[FSI]$ in the electrode (depicted in Figure 1a as Variable Proportion 1 in *x* wt%) and the quantity of Li^+ ions in $Li_x[C_2mpyr]_{1-x}[FSI]$ (referred to as Variable Proportion 2 in *y* mol%). For clarity, Variable Proportion 1 was referred to as the "$Li_x[C_2mpyr]_{1-x}[FSI]$ content" and Variable Proportion 2 was referred to as the "Li^+ concentration", even though the weight ratio of Li^+ ions in the composite electrode varied along with both evaluated proportions (as indicated in Table 1). Analyzing the influence of $Li_x[C_2mpyr]_{1-x}[FSI]$ content is crucial because it directly affects the binding properties of electrode ingredients. On the other hand, the Li^+ concentration is important because it influences the ionic conductivity and phase behavior of $Li_x[C_2mpyr]_{1-x}[FSI]$.

Both polymer-binder-containing (LFP−6w-PVDF) and polymer-binder-free (LFP−50w-Li0.01) cathode slurries were coated onto an aluminium current-collector sheet using three different wet gaps (*i.e.*, 100, 500, and 1,000 µm) to compare the binding ability of $Li_x[C_2mpyr]_{1-x}[FSI]$ with that of PVDF. As shown in Figure 1b, LFP−6w-PVDF slurry was successfully coated at a thickness of 100 µm without any cracking after drying. At 500 µm, the dried electrode showed small cracks throughout the entire coated layer and at 1000 µm, the cracks were more significant, and the underlying aluminium substrate was clearly visible in the cracked regions. The dried electrodes with these coating thicknesses (*i.e.*, 500 and 1000 µm) detached completely from the current collector when placed in a vertical position. In contrast, the dried polymer-binder-free LFP−50w-Li0.01 composite electrode remained intact for all three evaluated wet gaps. Although the surface roughness tended to increase with an increase in the wet gap, the dried LFP−50w-Li0.01 had no cracks (Figure 1c). This confirms that $Li_x[C_2mpyr]_{1-x}[FSI]$ can act as a binder to hold electrode ingredients together in a certain shape and, at some conditions, $Li_x[C_2mpyr]_{1-x}[FSI]$ can support higher electrode loading than PVDF without obvious mechanical failures of the electrode.

The effect of the two variables on the nominal areal capacity of the polymer-binder-free LFP−$Li_x[C_2mpyr]_{1-x}[FSI]$ composite electrode was evaluated (Figure 1d). Indeed, some of the evaluated $Li_x[C_2mpyr]_{1-x}[FSI]$ contents enabled coating at a 1,000-µm gap without a cracking issue after drying. The $Li_x[C_2mpyr]_{1-x}[FSI]$ contents resulting in unbroken thick electrodes are presented as the red region in Figure 1d. This region corresponds to the highest $Li_x[C_2mpyr]_{1-x}[FSI]$ content (*i.e.*, 50 wt%) regardless of the Li^+ concentration. The color bar on the right side in Figure 1d displays values of the nominal areal capacity, and they were obtained by the average of four electrodes of the same experiment. Considering the highest mass loading achieved (*i.e.*, ≈ 24.9 mg/cm^2) and the specific capacity of LFP (*i.e.*, 150 mAh/g, see Section 2.2.2 for details), it is possible to achieve a thick LFP−$Li_x[C_2mpyr]_{1-x}[FSI]$ composite electrode with a nominal areal capacity as high as 3.74 mAh/cm^2 (with 50 wt% $Li_x[C_2mpyr]_{1-x}[FSI]$). While only the highest $Li_x[C_2mpyr]_{1-x}[FSI]$ content supported a high areal capacity (using a coating gap of 1,000 um), all the polymer-binder-free LFP−$Li_x[C_2mpyr]_{1-x}[FSI]$ composite slurries were able to achieve an undamaged coating with a 100 µm wet gap, corresponding to a low nominal areal capacity in the color bar (*i.e.*, green region). This result highlights the binding ability of $Li_x[C_2mpyr]_{1-x}[FSI]$; it can function as a binder even at a relatively low weight ratio (*i.e.*, 15 wt%). When comparing the LFP loading values of the electrode prepared by the same wet gap (*i.e.*, 100 µm) at the fixed Li^+ concentration (*i.e.*, 1 mol%), the electrode with 50 wt% $Li_x[C_2mpyr]_{1-x}[FSI]$ (LFP−50w-Li0.01) had an LFP loading of 2.17 mg/cm², whereas it was measured to be 1.41 mg/cm² for 15 wt% $Li_x[C_2mpyr]_{1-x}[FSI]$ (LFP−15w-Li0.01). The LFP loading values of both polymer-binder-free LFP−$Li_x[C_2mpyr]_{1-x}[FSI]$ composite electrodes were different from that of LFP−6w-PVDF (which had a LFP loading of 1.71 mg/cm²). This difference in LFP loading, observed across all electrodes obtained using the same wet gap, is caused by the varying solid ratios in the different $Li_x[C_2mpyr]_{1-x}[FSI]$ contents tested. For instance, in the LFP-50w-Li0.01, less NMP was needed, resulting in a solid ratio of 60.1 wt%. Conversely, the

LFP-15w-Li0.01 slurry resulted in a solid ratio of 37.4 wt%.

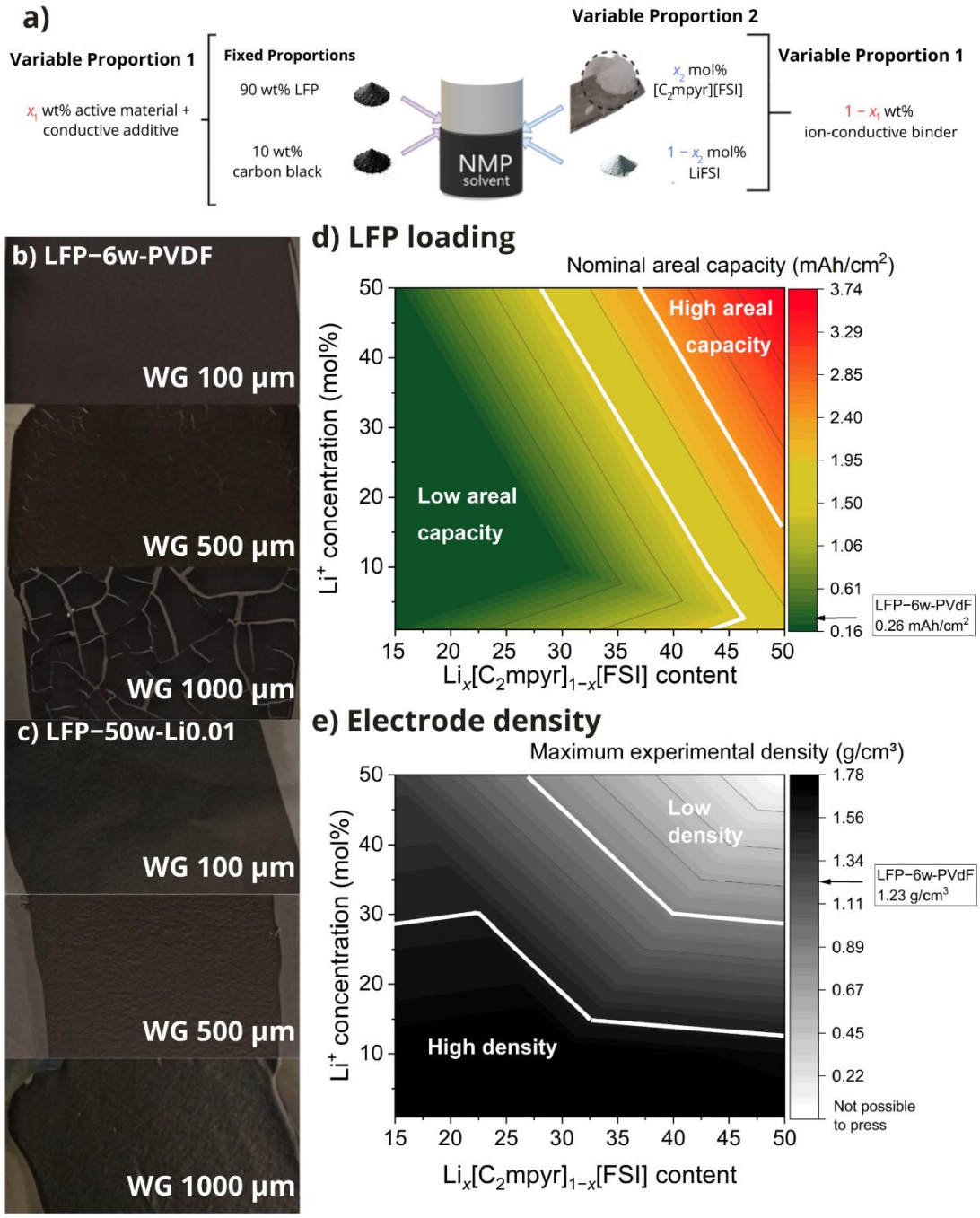

Figure 1. a) The formulation of a polymer-binder-free LFP−Li$_x$[C$_2$mpyr]$_{1-x}$[FSI] composite slurry with the two variable proportions. b,c) The photos of the dried surfaces of b) polymer-binder-containing electrodes (LFP−6w-PVDF) and c) polymer-binder-free electrodes (LFP−50w-Li0.01) on Al prepared using different wet gaps. d,e) Contour graphs for d) the calculated nominal areal capacity and e) the experimentally measured electrode density of polymer-binder-free LFP−Li$_x$[C$_2$mpyr]$_{1-x}$[FSI] composite electrodes on Al.

One might be concerned about a higher weight fraction of this non-polymer binder (*i.e.*, 15−50 wt% Li$_x$[C$_2$mpyr]$_{1-x}$[FSI]) than common proportions of polymer binders in LIBs (*e.g.*, typically ≈3 wt% for commercial applications[52]). However, it should be noted that Li$_x$[C$_2$mpyr]$_{1-x}$[FSI] does not work only as

a binder, but as an electrolytically functional material; indeed, $Li_x[C_2mpyr]_{1-x}[FSI]$ serves as an ionic conductor that facilitates ion transport through the cathode film[27]. Therefore, another important consideration is that LIB electrodes typically have 30−40 vol% of porosity[26], which is filled with a liquid electrolyte solution. If the density of a commercial electrolyte solution (LP30) is assumed to be 1.3 g/cm^3[53,54], the weight ratio of the electrolyte solution in an LFP cathode layer (with the same composition as LFP−6w-PVDF) in LIBs is estimated to be 20−32 wt%. Consequently, the $Li_x[C_2mpyr]_{1-x}[FSI]$ content ranging from 15 to 30 wt% is considered within commercially viable conditions, provided that $Li_x[C_2mpyr]_{1-x}[FSI]$ entirely replaces the electrolyte inside the cathode. In addition, 50 wt% $Li_x[C_2mpyr]_{1-x}[FSI]$ in the cathode layer would also be a comparable situation given the low electrode density of LFP−6w-PVDF after pressing (*i.e.*, 1.23 g/cm^3), which accounts 60.3 vol% of porosity allowing 62 wt% of LP30 in the cathode layer.

The polymer-binder-free LFP−$Li_x[C_2mpyr]_{1-x}[FSI]$ composite electrodes were also evaluated in terms of the experimentally achievable electrode density, as shown in Figure 1e. The electrode sheet of each studied formulation (with a coating gap of 100 μm) was punched into ϕ14 mm disks and compressed using a pellet die to produce the densified electrode. The electrodes (LFP−50w-Li0.50) with the highest content of $Li_x[C_2mpyr]_{1-x}[FSI]$ (*i.e.*, 50 wt%) and Li^+ ions (*i.e.*, 50 mol%) formed a soft film that was easily damaged and impossible to be compressed. SEM experiments (Supplementary Figure 1) show that the electrode surface of this formulation (LFP−50w-Li0.50) had a more plastic-crystal appearance than those of the other formulations. In addition, this condition showed a higher surface roughness than others and particles tended to form big chunks with wavy edges (which would visually prove that $Li_{0.50}[C_2mpyr]_{0.50}[FSI]$ stays as an amorphous solid phase in the composite electrode). These obvious differences are a result of a higher amount of $Li_x[C_2mpyr]_{1-x}[FSI]$ and its Li^+ concentration, providing the electrode with a greater volume of an amorphous phase (that is easily deformed by external pressure) than others[55]. It is known that the physical state of $Li_x[C_2mpyr]_{1-x}[FSI]$ at room temperature changes from solid (*i.e.*, OIPC) to solid + liquid to liquid (*i.e.*, IL) along with an increase in the Li^+ concentration (≤50 mol%)[38,56]. In other words, $Li_x[C_2mpyr]_{1-x}[FSI]$ becomes soft as the Li^+ concentration increases[38], which reduces the binding ability of $Li_x[C_2mpyr]_{1-x}[FSI]$. Furthermore, an increase in the $Li_x[C_2mpyr]_{1-x}[FSI]$ content means increasing the weight fraction of a softer material (than LFP and carbon-black particles) in the electrode, which also decreases the rigidness of the composite electrode. Therefore, even though LFP−50w-Li0.50 supports the highest nominal areal capacity, this condition seems impractical to offer high volumetric energy density as the electrode for LIBs and it is not suitable to be applied to electrode manufacturing (whose steps have been conventionally done in roll-to-roll, which require enough mechanical strength of electrode layers to process).

From Figure 1e, the other three corners of the two Variable Proportions (except for the top right corner; *i.e.*, LFP−50w-Li0.01, LFP−15w-Li0.01, and LFP−15w-Li0.50) are worth investigating further. As LFP−50w-Li0.01 was able to provide both high nominal areal capacity and high electrode density, this composite electrode was studied for high-energy-density applications (Section 3.3.1). On the other hand, both LFP−15w-Li0.01 and LFP−15w-Li0.50 were suitable to generate compressible electrodes with a coating gap of 100 μm even though the amount of $Li_x[C_2mpyr]_{1-x}[FSI]$ was relatively low. For them, half-cell tests were performed to evaluate the effect of the Li^+ concentration on their electrochemical performance (Section 3.3.2).

3.2. Homogeneity and solubility of the polymer-binder-free LFP−$Li_x[C_2mpyr]_{1-x}[FSI]$ composite electrode

The uniform distribution of electrode ingredients (especially for electron- and ion-conductive materials) in the electrode layer is important to maximize the electrochemical performance of the electrode[38]. Therefore, the dispersibility of the ingredients in the polymer-binder-free LFP−$Li_x[C_2mpyr]_{1-x}[FSI]$ composite electrode was evaluated before the cell-cycling tests. LFP−50w-Li0.01 with the highest nominal areal capacity was chosen for the analysis by means of surface and cross-section SEM, whose

results are presented in Figures 2a and 2b, respectively. The surface image appears to be flat and sufficiently uniform without any localized materials (*e.g.*, OIPC-electrolyte grains that would form during drying an electrode slurry[23]). The image also has relatively dark regions with blurred particle edges. These indicate that 50 wt% $Li_{0.01}[C_2mpyr]_{0.99}[FSI]$ helped the deformation of the electrode while under compression and filled the pores to connect particles. The cross-sectional image shows almost the same appearance as the surface image. Although the image contains some artifacts generated by cutting the electrode (*e.g.*, diagonal lines that run at *ca*. 30° from the line of the current-collector surface and a particle attached to the cross-sectional surface), the densification of the electrode layer towards the current collector is clearly seen; no pores are observed at the bottom region of the electrode. This further highlights the excellent deformability of $Li_{0.01}[C_2mpyr]_{0.99}[FSI]$ against external pressure. These images strengthen the idea that the complete replacement of a liquid electrolyte solution in the pores of the LIB electrode (*i.e.*, exclusion of unfilled pores) might be possible by employing a sufficient amount of $Li_x[C_2mpyr]_{1-x}[FSI]$ as an ion-conductive binder. If the amount of $Li_x[C_2mpyr]_{1-x}[FSI]$ is relatively small (*i.e.*, ≤30 wt%), some pores in the electrode likely remain unfilled, but such conditions still can provide effective ion-conduction pathways (that presumably expand along with the particle surfaces) throughout the electrode layer (especially if they are percolated)[23,38].

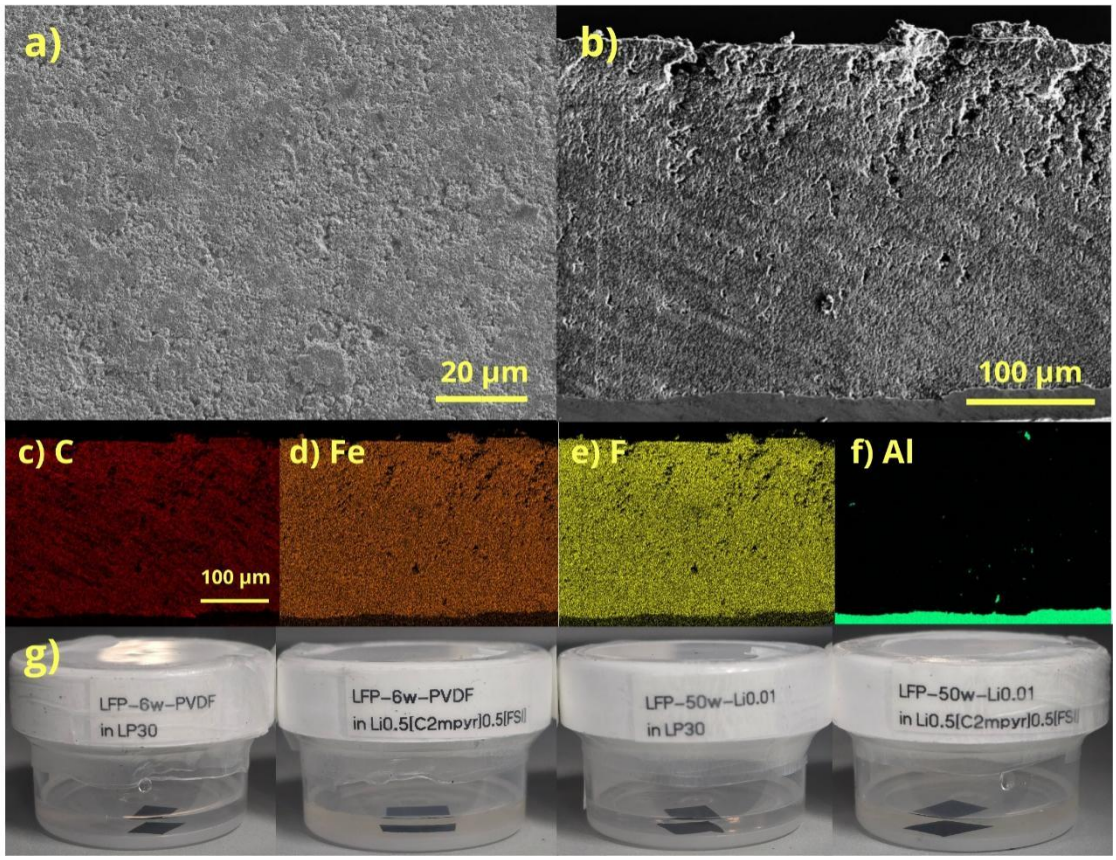

Figure 2. a) Surface and b) cross-sectional SEM images of LFP−50w-Li0.01 on Al current collector. EDX elemental mappings of c) C, d) Fe, e) F, and f) Al, for the area resolved in b). g) Pictures of LFP−6w-PVDF (first and second samples, from left to right) and LFP−50w-Li0.01 (third and fourth samples) pieces in LP30 and $Li_{0.50}[C_2mpyr]_{0.50}[FSI]$ after stored in an oven at 50 °C for >16 h.

To provide insights into the dispersibility of the electrode ingredients further, EDX was performed for the same cross-section as Figure 2b. The excellent dispersibility was proven by elemental mapping, showing that carbon (Figure 2c, mainly contributed by carbon black and $[C_2mpyr]^+$), iron (Figure 2d, originating from LFP), and fluorine (Figure 2e, sourced from $[FSI]^-$) are well distributed within the electrode layer. No localized electrode ingredients are resolved. The result clarifies that the "*all-in-one*" method using

NMP can provide the electrode layer with a better distribution of the ingredients than that using water and a secondary solvent[23,38]. This is likely to be due to the high solubility of $Li_x[C_2mpyr]_{1-x}[FSI]$ in NMP and the use of only one solvent, both of which tend to restrict the isolation of $Li_x[C_2mpyr]_{1-x}[FSI]$ from particle surfaces while evaporating NMP. Some pieces of aluminum were detected on the surface of the cross-section (Figure 2f), which confirmed the presence of artefacts stemming from the electrode-cutting process, but they did not affect the evaluation of the dispersibility of the electrode ingredients.

Additionally, to check the stability of the coated layer, some solubility tests were conducted at 50 °C. The solubilities of both polymer-binder-containing (LFP−6w-PVDF) and polymer-binder-free (LFP−50w-Li0.01) electrodes in a commercial electrolyte solution (*i.e.*, LP30) and IL (*i.e.*, $Li_{0.50}[C_2mpyr]_{0.50}[FSI]$ which are comprising the same ionic constitutes as the ion-conductive binder in the electrode) were compared. LFP−6w-PVDF remained intact in both liquids, as indicated by the achromatic color of the liquids (Figure 2g). Similarly, LFP−50w-Li0.01 did not break apart in both liquids; LFP−50w-Li0.01 was stable for at least 2 weeks. To avoid using different anions in the cathode (*i.e.*, $[FSI]^-$) and separator layers (*i.e.*, PF_6^-), the subsequent battery tests for polymer-binder-free LFP−$Li_x[C_2mpyr]_{1-x}[FSI]$ composite electrodes were conducted using a polyolefin separator filled with $Li_{0.50}[C_2mpyr]_{0.50}[FSI]$.

3.3. Cell performances of polymer-binder-free LFP−$Li_x[C_2mpyr]_{1-x}[FSI]$ composite electrodes

3.3.1. Electrodes for high-energy-density applications

LFP−50w-Li0.01 with a high nominal areal capacity (LFP loading: 11.7 mg/cm^2) was used for battery evaluation in an LMB configuration (with an interlayer filled with $Li_{0.50}[C_2mpyr]_{0.50}[FSI]$). Its cell test showed the expected charge/discharge profile of LFP, *i.e.*, intercalation/deintercalation processes at around 3.4 V *vs*. Li/Li$^+$[51], as seen in Figure 3a by the characteristic two-phase plateau of Fe^{2+} and Fe^{3+} in the LFP crystal. However, its discharge capacity was lower than the theoretical value of LFP (170 mAh/g)[57,58]: 135.7 mAh/g for the first cycle and 128.9 mAh/g for the 13th cycle. The same LFP was tested for the regular formulation with PVDF (*i.e.*, LFP−6w-PVDF) in LP30 and showed a discharge capacity of 155.9 mAh/g (Supplementary Figure 2). This confirms that the maximum achievable capacity of this LFP is <170 mAh/g, which is because this material is carbon-coated for conductivity improvement (indeed, the supplier certifies its capacity is >154 mAh/g). In addition, LFP−6w-PVDF in $Li_{0.50}[C_2mpyr]_{0.50}[FSI]$ was tested, resulting in an additional loss of 9 mAh/g of the discharge capacity (Supplementary Figure 2). This means that even if the commercial polymer-binder formulation is employed, only 146.9 mAh/g can be obtained for our setup. Therefore, the capacity reduction that can be ascribed to our new cathodes (*e.g.*, LFP−50w-Li0.01) is about 10−15 mAh/g, which can be related to the use of $Li_x[C_2mpyr]_{1-x}[FSI]$ as an ion-conductive binder in the electrode.

The charge and discharge profiles of LFP−50w-Li0.01 present a high overvoltage, *e.g.,* a voltage difference between the charge and discharge plateaus of >0.1 V. This was probably caused by a thick layer of this electrode, which increases diffusion polarization within the electrode layer and increases resistance[59]. To clearly evaluate the overvoltage, a dQ/dV analysis was conducted. A pair of sharp dQ/dV peaks appears with a peak height of 3.0 ± 0.5 Ah/gV (Figure 3b). The differences between peak voltages were estimated to be 0.12 V for the first cycle, 0.13 V for the fifth cycle, and 0.16 V for the 13th cycle, which increased with an increase in the cycle number. This suggests that the cell resistance gradually increases over cycling, which is likely to be due to the rearrangement of LFP and carbon-black particles induced by the volume change of the active materials during cycling. This would cause the gradual disconnection of LFP particles from the electron- and ion-conductive networks in the electrode layer. Both contribute to a decrease in the observable capacity as the cycle test progresses.

Indeed, the charge/discharge capacities of LFP−50w-Li0.01 in $Li_{0.50}[C_2mpyr]_{0.50}[FSI]$ decreased over

cycling (Figure 3c); the capacity loss during cycling was estimated to be 1.9% from the first to fifth cycles and 3.2% from the fifth to 13th cycle. Conversely, the capacity loss for LFP−6w-PVDF in $Li_{0.50}[C_2mpyr]_{0.50}[FSI]$ was negligible from the first to fifth cycles and 0.7% from the fifth to 13th cycles (Supplementary Figure 3a), which is considerably lower than LFP−50w-Li0.01. This implies that the binding ability of $Li_x[C_2mpyr]_{1-x}[FSI]$ to hold the electrode structure during cycling would be enough for multiple cycles but it would not be as strong as PVDF. However, it should be noted that this deduction is from the comparison between different LFP-loading values (*i.e.*, 11.7 mg/cm^2 for LFP−50w-Li0.01 *vs.* 2.04 mg/cm^2 for LFP−6w-PVDF) as well and LFP−6w-PVDF could not reach a comparable loading value of >10 mg/cm^2 (*i.e.*, a wet gap of >500 µm, as discussed in Section 3.1). Therefore, polymer-binder-free formulations are still effective in offering cell cycling with a relatively high LFP loading that cannot be reached by conventional polymer-binder-containing formulations.

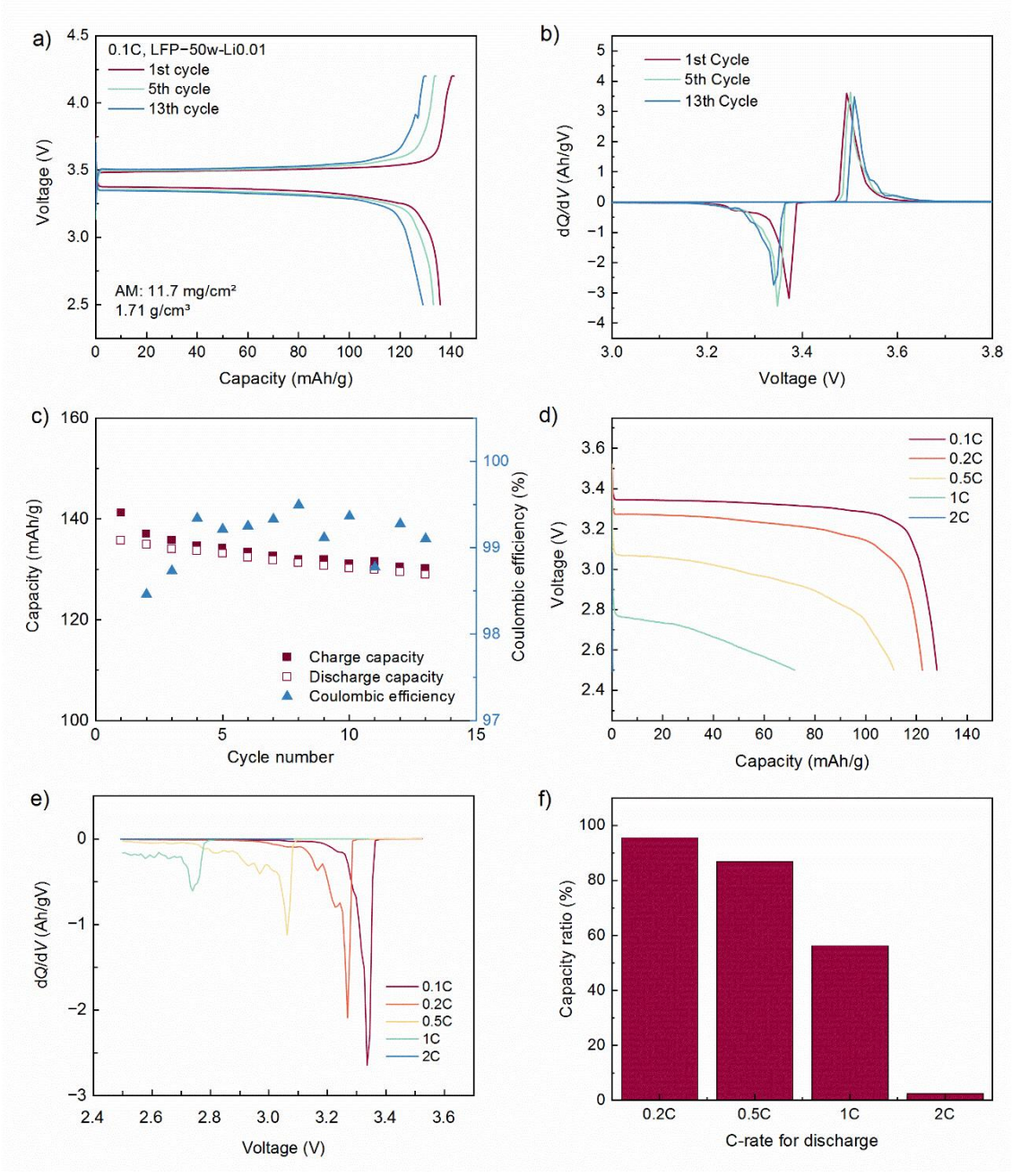

Figure 3. The results of the battery tests for the high-energy-density polymer-binder-free LFP−$Li_x[C_2mpyr]_{1-x}[FSI]$ composite cathode (LFP−50w-Li0.01) on Al paired with Li metal in

DOI: 10.20517/scierxiv202408.01.v1

$Li_{0.50}[C_2mpyr]_{0.50}[FSI]$ at 50 °C. a) The charge/discharge profiles of LFP−50w-Li0.01 at 0.1C at the selected cycles. b) The dQ/dV profiles of LFP−50w-Li0.01 at 0.1C at the selected cycles. c) The charge/discharge capacities and Coulombic efficiency of LFP−50w-Li0.01 for 13 cycles at 0.1C. d) The voltage profiles of LFP−50w-Li0.01 during the discharge step under different C-rates from 0.1C to 2C. e) The dQ/dV profiles of LFP−50w-Li0.01 during discharging at different C-rates. f) The discharge capacity ratios of LFP−50w-Li0.01 for different C-rates (where the discharge capacity at 0.1C was set as 100%).

As for the Coulombic efficiency, both LFP−50w-Li0.01 and LFP−6w-PVDF in $Li_{0.50}[C_2mpyr]_{0.50}[FSI]$ showed different behavior over cycling. The Coulombic efficiency of LFP−50w-Li0.01 (in Figure 3c) gradually increased from 98.5% at the first cycle to 99.4% at the fourth cycle. After that, it fluctuated ≈99%. In contrast, the Coulombic efficiency of LFP−6w-PVDF was 94.2% at the first cycle and around 97% for the subsequent cycles (Supplementary Figure 3b). Generally, a higher irreversible capacity and lower Coulombic efficiency are expected at the first cycle than subsequent cycles, which is due to the cathode electrolyte interphase (CEI) formation[60]. However, the Coulombic efficiency at the subsequent cycles should be as close as 100%, otherwise, it might indicate some irreversible phenomena, *e.g.*, the continuous CEI formation and loss of an active material over cycling. It is noteworthy that, at the 13th cycle, the Coulombic efficiency of LFP−50w-Li0.01 was *ca*. 2% higher than that of LFP−6w-PVDF. This implies that, although the irreversible phenomena are present in both cases, LFP−50w-Li0.01 is more stable than LFP−6w-PVDF. The result suggests that the combination of $Li_{0.50}[C_2mpyr]_{0.50}[FSI]$ and PVDF contributes to a relatively large irreversible capacity (*i.e.*, a decrease in the Coulombic efficiency), which would be related to the dehydrofluorination of PVDF reported on the anode side[23].

When LFP−50w-Li0.01 is tested at high discharge currents, its discharge capacity at 1C decreases to 56% of that measured at 0.1C and it cannot perform a sufficient discharge over currents of 2C or higher, as shown in Figures 3d and 3f. Although the previous study suggested that increasing the electrode loading potentially decreases the internal resistance of an electrode layer by an increased number of parallel connections (*i.e.*, electron-conduction pathways along the direction parallel with the current-collector surface)[59], the discharge rate capability of LFP−50w-Li0.01 implied that another increase in the resistance negated such a positive effect because of the elongated electronic and ionic pathways (along the normal to the current-collector surface) in thick electrodes. The addition of $Li_x[C_2mpyr]_{1-x}[FSI]$ to the electrode was expected to decrease ionic resistance, but it appears that the electronic resistance still limited the achievable capacity at high-current tests. Figure 3e illustrates the significant changes in the lithiation voltage of LFP (*i.e.*, the dQ/dV-peak voltage) and in its lithiation amount (*i.e.*, the area of dQ/dV signal) when cycled at higher currents. These changes can be caused by the dependency on rate of Li^+ transport. In cases where there are some kinetic constraints, such as poor conductivity or slow diffusion rates, the lithium-ion transport in the electrode is restricted[61]. This phenomenon would allow for the emergence of additional small peaks (following the main dQ/dV peak) that were not observed at 0.1C discharging, although another possibility of the small peaks is noise that was not sufficiently removed because of the sampling rate in this study (*i.e.*, the instrument took a datapoint every 20-mV difference).

The results of high-rate discharge tests for LFP−50w-Li0.01 suggest this electrode is not adequate for high-power applications, but it is ideal for high-energy applications. This electrode demonstrated the actual areal capacity of up to 1.75 mAh/cm². As LFP−50w-Li0.01 can provide the nominal areal capacity of up to 3.74 mAh/cm² (Figure 1d), a further increase in the actual areal capacity of this polymer-binder-free cathode in the LMB configuration is possible. However, the half-cell experiments using the electrode with the nominal areal capacity of >2.0 mAh/cm^2 are challenging. A preliminary test of LFP−50w-Li0.01 with the nominal areal capacity of 2.67 mAh/cm^2 (LFP loading: 17.86 mg/cm^2) suffered from voltage fluctuations during charging (as seen in Supplementary Figure 4), which might indicate micro shorts stemming from Li dendrite formation[62]. Nevertheless, this electrode showed the first discharge capacity of 139.4g mAh/g, which was equivalent to 2.49 mAh/cm^2, demonstrating the excellent workability of the polymer-binder-free cathode for high-energy applications. Further optimization of the anode (*e.g.*, engineering Li-metal anode[63] and using other anode active materials

that are compatible with $Li_x[C_2mpyr]_{1-x}[FSI]$[23,38]) and separator (*e.g.*, ceramic coating on polyolefin separators[64-66] and the use of ceramic separators[67]) is beneficial to prevent the aforementioned micro-short issue for stable cycling of the batteries employing polymer-binder-free LFP−$Li_x[C_2mpyr]_{1-x}[FSI]$ composite cathodes with a high areal capacity.

3.3.2. Electrodes for high-power-density applications

The two polymer-binder-free LFP−$Li_x[C_2mpyr]_{1-x}[FSI]$ composite cathodes with 15 wt% $Li_x[C_2mpyr]_{1-x}[FSI]$ (*i.e.*, LFP−15w-Li0.01 and LFP−15w-Li0.50) were selected for battery tests with limited LFP loading (*i.e.*, the nominal areal capacity of 0.2−0.3 mAh/cm², which is in the same range as LFP−6w-PVDF). As discussed in Section 3.1, these conditions could not provide a nominal areal capacity of >1.0 mAh/cm^2 because of the low $Li_x[C_2mpyr]_{1-x}[FSI]$ content. However, these are the conditions that would offer the best compromise between the maximum weight ratio of LFP in the electrode and the lowest possible mechanical strength of the electrode for cell operation. Therefore, battery cycling experiments were performed to show their potential for providing a high power density (*i.e.*, a high capacity at a high current).

In charge/discharge-rate tests at 2C, two Li^+ concentrations were compared. LFP−15w-Li0.01 exhibited lower overvoltages in both charge and discharge curves than LFP−15w-Li0.50, resulting in a higher specific capacity (Figures 4a and 4c). The overvoltage is due to three factors: IR loss, activation polarization, and concentration polarization[68]. The immediate voltage jump caused by applying a current refers to the IR loss and the subsequent voltage change to initiate lithiation/delithiation reactions is considered the activation polarization, while the voltage change at the end of charging/discharging reactions is related to concentration polarization. An increase in both Ohmic loss and activation polarization from LFP−15w-Li0.01 to LFP−15w-Li0.50 suggests that the electric resistance of the polymer-binder-free LFP−$Li_x[C_2mpyr]_{1-x}[FSI]$ composite cathode rises as the Li^+ concentration increases in its formulation. This implies that $Li_{0.50}[C_2mpyr]_{0.50}[FSI]$ (which is an IL) covers carbon-black particles more significantly than $Li_{0.01}[C_2mpyr]_{0.99}[FSI]$ (which is regarded as a solid composite), providing LFP−15w-Li0.50 with a more tortuous electron-conduction pathways than LFP−15w-Li0.01. This consideration is supported by the previous study, which reported an increased charge-transfer resistance at the interface between Si and $Li_{0.50}[C_2mpyr]_{0.50}[FSI]$ when carbon-black particles were preferentially covered by $Li_{0.50}[C_2mpyr]_{0.50}[FSI]$ [38]. Furthermore, a higher concentration polarization was observed for LFP−15w-Li0.50 than for LFP−15w-Li0.01. This indicates that a greater amount of Li^+ ions available within the electrode does not necessarily lead to an improvement in mass transfer. A highly Li^+-concentrated interface is not favorable for LFP to progress its delithiation as it would lead to the formation of relatively immobile LiFSI because of the solubility limit of Li^+ in $Li_x[C_2mpyr]_{1-x}[FSI]$ at the LFP surface, resulting in a large concentration polarization [69]. As the discharge (lithiation) step comes after the charge (delithiation) step, the aforementioned issue might also affect the efficacy of LFP delithiation.

Superior charge/discharge rate capabilities of LFP−15w-Li0.01 to LFP−15w-Li0.50 were clarified in detail as the capacity ratios at different C-rates. The capacity-ratio values for both lithiation (Figure 4b) and delithiation (Figure 4d) clarify that LFP−15w-Li0.01 can offer a higher capacity than LFP−15w-Li0.50 at a high current. For instance, at a 2C current, the 0.1C capacity of LFP−15w-Li0.01 retained 97.2% for lithiation and 94.6% for delithiation, whereas LFP−15w-Li0.50 showed a capacity ratio of 81.4% for lithiation and 76.5% for delithiation. Therefore, a polymer-binder-free LFP−$Li_x[C_2mpyr]_{1-x}[FSI]$ composite cathode with a lower Li^+-concentration in $Li_x[C_2mpyr]_{1-x}[FSI]$ is more useful for high-power-density applications.

The cycle performances of these electrodes were also evaluated at 0.1C. Both electrodes show a continuous decrease in the capacity as the cycle number increases (Figures 4e and 4f). However, an

obvious difference in the degradation speed was found. LFP−15w-Li0.01 experienced a loss of a *ca.* 6-mAh/g capacity after 80 cycles, while *ca.* 15 mAh/g was lost for LFP−15w-Li0.50 through the same cycling period. This result suggests that a polymer-binder-free LFP−$Li_x[C_2mpyr]_{1-x}[FSI]$ composite cathode with a softer $Li_x[C_2mpyr]_{1-x}[FSI]$ (*e.g.*, LFP−15w-Li0.50 *vs*. LFP−15w-Li0.01) becomes more susceptible to the structural deformation of the cathode because of the volume expansion/shrinkage of LFP particles, resulting in losing a greater amount of active LFP particles over cycling. Therefore, to maximize the cyclability of the polymer-binder-free LFP−$Li_x[C_2mpyr]_{1-x}[FSI]$ composite cathode, choosing a low Li^+ concentration (*e.g.*, 1 mol%) is beneficial. In addition, as shown in Supplementary Figure 5, the discharge capacity retention of LFP−15w-Li0.01 was close to that of LFP−6w-PVDF and LFP−15w-Li0.01 showed higher Coulombic efficiency than LFP−6w-PVDF (except for the first cycle), which demonstrates a possibility for the polymer-binder-free approach in achieving the promising electrochemical performance comparable with of polymer-binder-containing LFP cathodes.

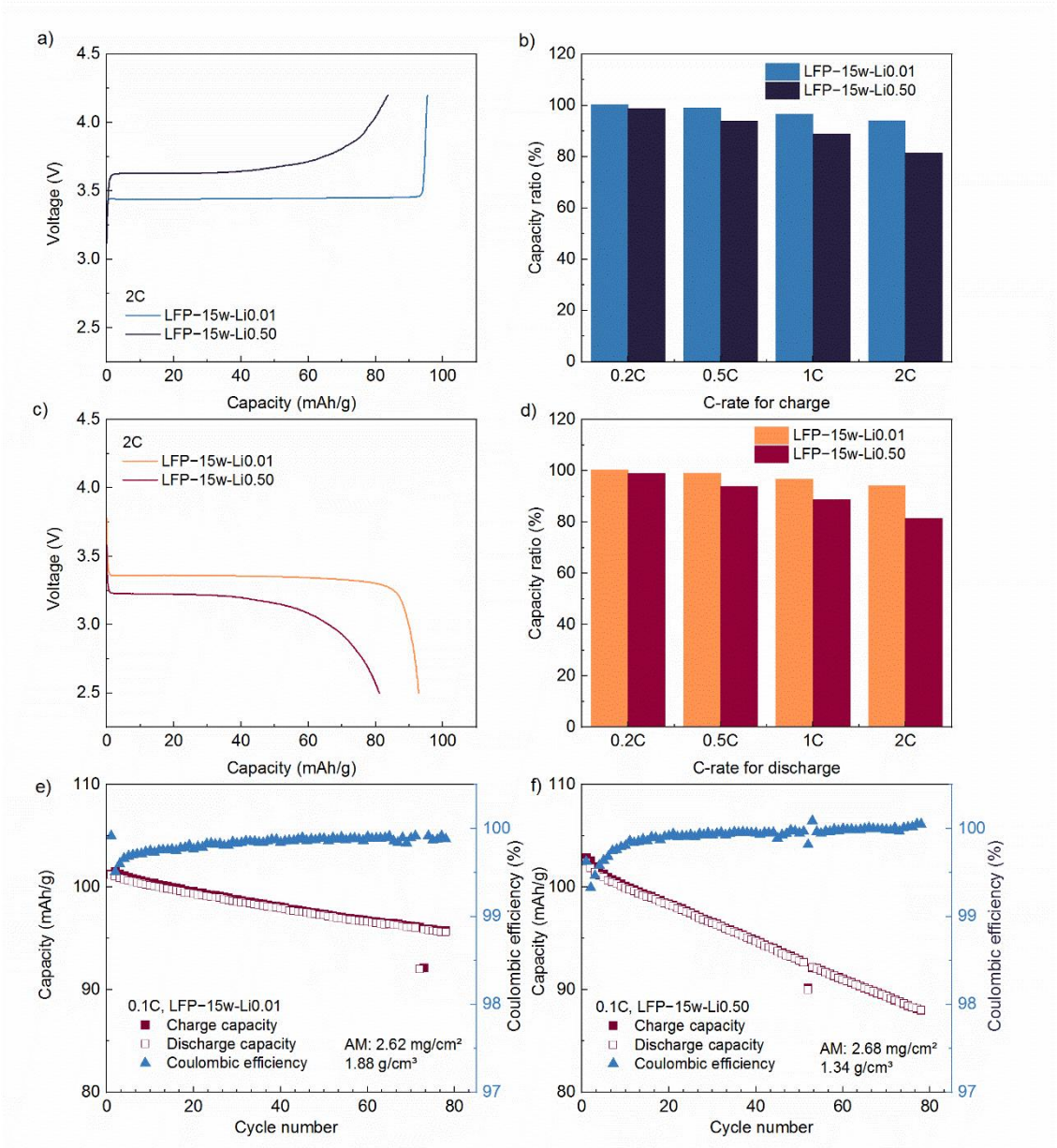

Figure 4. The results of the battery tests for high-power-density polymer-binder-free LFP−$Li_x[C_2mpyr]_{1-x}[FSI]$ composite cathodes (LFP−15w-Li0.01 and LFP−15w-Li0.50) paired with Li metal in $Li_{0.50}[C_2mpyr]_{0.50}[FSI]$ at 50 °C. a) The voltage profiles of LFP−15w-Li0.01 and LFP−15w-Li0.50 during the charge step at 2C. b) The charge capacity ratios of LFP−15w-Li0.01

DOI: 10.20517/scierxiv202408.01.v1

and LFP−15w-Li0.50 for different C-rates (where the charge capacity at 0.1C was set as 100%). c) The voltage profiles of LFP−15w-Li0.01 and LFP−15w-Li0.50 during the discharge step at 2C. d) The discharge capacity ratios of LFP−15w-Li0.01 and LFP−15w-Li0.50 for different C-rates (where the discharge capacity at 0.1C was set as 100%). e,f) The charge/discharge capacities and Coulombic efficiencies of e) LFP−15w-Li0.01 and f) LFP−15w-Li0.50 for 80 cycles at 0.1C.

As for the change in the Coulombic efficiency over cycling, both electrodes also show different behaviors (Figures 4e and 4f). Although LFP−15w-Li0.01 had a higher Coulombic efficiency than LFP−15w-Li0.50 at the first few cycles, its stabilization for LFP−15w-Li0.01 takes a considerably longer cycle period than that for LFP−15w-Li0.50. A gradual increase in the Coulombic efficiency of Li^+-containing OIPC-based electrodes was previously referred to as "preconditioning"[23,38], whose origins have been discussed based on Joule heating[27] as well as the restructuring of the OIPC interface[70], and took *ca*. 20 cycles to be stabilized[23]. The Coulombic efficiency of LFP−15w-Li0.50 was almost stabilized after 20 cycles and, after that, it increased very slowly over cycling, reaching 99.99% at the 70th cycle and 100.1% at the 80th cycle, which evidence degradation processes after long cycling. In contrast, LFP−15w-Li0.01 did not show an obvious stabilization of the Coulombic efficiency after around 20 cycles; it kept increasing over cycling but still remained at a lower level (*i.e.*, 99.8%) than that of LFP−15w-Li0.50 after 80 cycles. This difference is reasonable as a harder ion-conductive binder (*i.e.*, $Li_{0.01}[C_2mpyr]_{0.99}[FSI]$) is expected to take a longer period than a softer one (*i.e.*, $Li_{0.50}[C_2mpyr]_{0.50}[FSI]$) to expand throughout the LFP-particle surfaces and form CEI. Nevertheless, both electrodes showed enough levels of reversibility of lithiation/delithiation reactions for multiple decades of cycles.

3.3.3. Full-cell demonstration using the polymer-binder-free cathode and an intercalation-type anode

In this last experimental section, the compatibility of the polymer-binder-free LFP−$Li_x[C_2mpyr]_{1-x}[FSI]$ composite cathode with rechargeable batteries using a non-alkali-metal anode was evaluated. The stable cycling of such full cells is challenging as there are no excessive Li^+ sources available in the cells, which differs from the LMB configuration (where Li^+ ions can be provided from Li metal excessively) discussed previously. To maximize the energy density and cyclability of the batteries, the use of graphite on the anode side is preferred. However, IL-based electrolytes often suffer from the poor cyclability of graphite, which requires an SEI-forming additive to facilitate the reversible Li^+ intercalation/deintercalation[71-73], or the constituent ions need to be modified[74]. Meanwhile, $Li_{0.10}[C_2mpyr]_{0.90}[FSI]$ is reportedly compatible with graphite and supports its stable cycling[23]. Therefore, graphite−$Li_{0.10}[C_2mpyr]_{0.90}[FSI]$ composite anode was employed for full-cell measurements. As this electrode undergoes a large irreversible reaction at the first cycle [23], it was preconditioned in a solid-state half cell and then the preconditioned graphite−$Li_{0.10}[C_2mpyr]_{0.90}[FSI]$ composite anode was paired with fresh LFP−15w-Li0.10 in $Li_{0.50}[C_2mpyr]_{0.50}[FSI]$ for demonstration (see Section 2.2.1 for the detailed procedure of cell assembly).

Figure 5a shows the charge/discharge profile of a preconditioned graphite−$Li_{0.10}[C_2mpyr]_{0.90}[FSI]$ | LFP−15w-Li0.10 cell at the first cycle. This full cell showed a discharge capacity compatible with battery tests of polymer-binder-free LFP−$Li_x[C_2mpyr]_{1-x}[FSI]$ composite cathodes in the LMB configuration (*e.g.*, Figures 4e and 4f), but the Coulombic efficiency for the first cycle was only 58%. The poor Coulombic efficiency cannot be attributed only to the SEI formation on graphite as this process is speculated to have almost progressed during the first three cycles in a half-cell configuration. Because the first Coulombic efficiency of polymer-binder-free LFP−$Li_x[C_2mpyr]_{1-x}[FSI]$ composite cathodes was evaluated to be >98% (*e.g.*, Figures 3c, 4e, and 4f), this irreversible capacity of the full cell appears to be originated from the preconditioned graphite−$Li_{0.10}[C_2mpyr]_{0.90}[FSI]$ side. As $Li_{0.10}[C_2mpyr]_{0.90}[FSI]$ (coming from the interlayer) and $Li_{0.10}[C_2mpyr]_{0.90}[FSI]$ (in the graphite-anode layer) are miscible, the low first Coulombic efficiency would imply a partial rupture of the pre-formed SEI on graphite,

requiring the irreversible electrochemical reaction to rebuild it. The subsequent cycles showed improved Coulombic efficiency, but the achievable capacity decreased with an increase in the cycle number. This is likely to be because of the capacity mismatch between the preconditioned graphite−$Li_{0.10}[C_2mpyr]_{0.90}[FSI]$ anode and LFP−15w-Li0.10 developed as the cycle number increases.

To provide further insights into the reversibility of electrochemical reactions on both electrodes, dQ/dV analysis was performed. Figure 5b depicts four dQ/dV peaks in the charge step and five dQ/dV peaks in the discharge step. A peak in this type of graph shows the equilibrium between different electrochemically active phases [75] and can inform the progress of electrochemical reactions on both electrodes separately if the two successive peaks are separated well. As discussed before for the polymer-binder-free LFP−$Li_x[C_2mpyr]_{1-x}[FSI]$ composite cathode in the LMB configuration, the narrow oxidation peak at 3.46 V corresponds to the deintercalation of Li^+ ions from LFP, while the reduction peak at 3.40 V is the intercalation of Li^+ ions to LFP[61]. On the other hand, the broader peaks at 3.24, 3.34, and 3.37 V for oxidation and 3.17, 3.28, and 3.32 V for reduction are related to the intercalation/deintercalation of Li^+ ions on the graphite side[61] and each pair of dQ/dV peaks is assigned to the transition from one stage structure to another[76,77]. The origin of the dQ/dV peak at 3.22 V for the reduction process has yet to be fully understood, but some types of graphite (*e.g.*, mesocarbon microbeads) are known to show this additional dQ/dV peak during their delithiation[78-80]. From the comparison between the total area of dQ/dV processes during lithiation and that during delithiation for graphite, it was found that a large part of irreversible capacity was consumed on the graphite side at the full-cell voltage of 3.15−3.42 V and the irreversible reaction was concurrent with multiple Li^+-ion intercalation steps of graphite. Conversely, the total area of the dQ/dV process during lithiation and that during delithiation for LFP were almost the same as each other, suggesting the excellent reversibility of lithiation/delithiation reactions of LFP covered by $Li_{0.10}[C_2mpyr]_{0.90}[FSI]$.

Although engineering the anode and electrolyte is required to improve the cyclability, this study successfully demonstrated the initial stage of the full-cell operation of rechargeable batteries comprising the polymer-binder-free LFP−$Li_x[C_2mpyr]_{1-x}[FSI]$ composite cathode and graphite anode. This lays the strong foundation for future studies on Li^+-containing OIPC-based batteries using a polymer-binder-free approach. Such batteries will be most likely to be solid-state batteries, thereby minimizing the structural-deformation-induced capacity decay of polymer-binder-free electrodes for better cyclability.

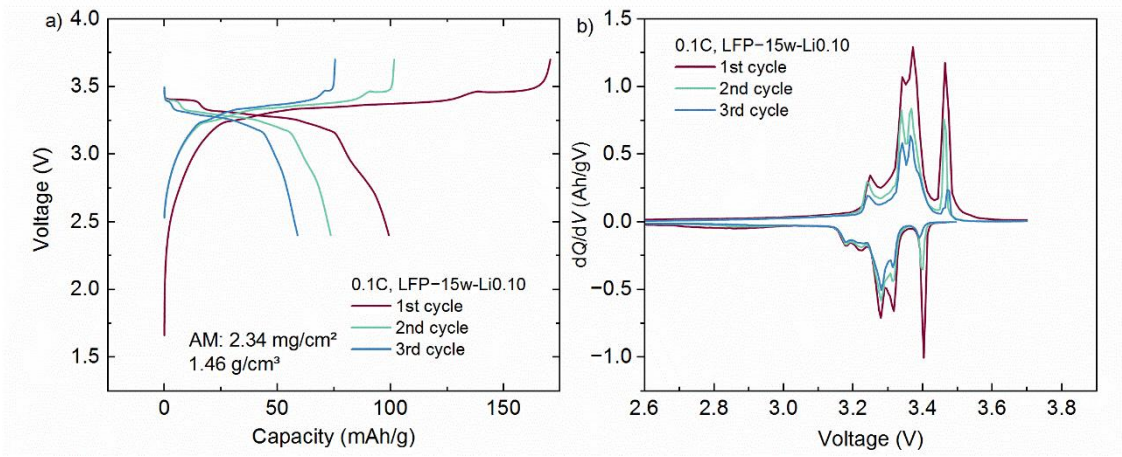

Figure 5. Full-cell demonstration of the polymer-binder-free LFP−$Li_{0.10}[C_2mpyr]_{0.90}[FSI]$ composite cathode (LFP−15w-Li0.10) paired with a graphite−$Li_{0.10}[C_2mpyr]_{0.90}[FSI]$ anode in $Li_{0.50}[C_2mpyr]_{0.50}[FSI]$ at 50 °C. a) The voltage profiles of a graphite−$Li_{0.10}[C_2mpyr]_{0.90}[FSI]$ | LFP−15w-Li0.10 cell for the first three cycles at 0.1C. b) The dQ/dV profiles of the graphite−$Li_{0.10}[C_2mpyr]_{0.90}[FSI]$ | LFP−15w-Li0.10 cell for the first cycle at 0.1C.

4. CONCLUSIONS

We created polymer-binder-free LFP electrodes using $Li_x[C_2mpyr]_{1-x}[FSI]$ as an ion-conductive binder. The effect of the weight ratio of $Li_x[C_2mpyr]_{1-x}[FSI]$ in the electrode and the Li^+ concentration in this ion-conductive binder on the electrode-manufacturing parameters (*i.e.*, the achievable nominal areal capacity and the maximum electrode density without breaking the electrode layer) was studied to overcome the electrode-loading limitation using conventional polymer-binder-containing electrode formulation as well as to provide functional polymer-binder-free LFP−$Li_x[C_2mpyr]_{1-x}[FSI]$ composite electrodes for both high-energy-density and high-power-density batteries. We clarified that a polymer-binder-free approach can offer a higher nominal areal capacity than a conventional approach using PVDF as a (non-conductive) binder for LFP and the highest $Li_x[C_2mpyr]_{1-x}[FSI]$ content of 50 wt% enabled the generation of crack-free high-loading LFP electrodes with a nominal areal capacity of ≤3.74 mAh/cm^2, which is suitable for high-energy-density batteries. On the other hand, the $Li_x[C_2mpyr]_{1-x}[FSI]$-deficient condition (*i.e.*, 15 wt% $Li_x[C_2mpyr]_{1-x}[FSI]$) provided the electrodes with a high LFP weight ratio and sufficient mechanical integrity at a low electrode-loading value and, therefore, such electrodes were tested for high-power-density batteries.

A polymer-binder-free LFP composite electrode with 50 wt% $Li_{0.01}[C_2mpyr]_{0.99}[FSI]$ showed the uniform distribution of electrode ingredients as well as moderate endurance against the structural deformation in the IL, $Li_{0.50}[C_2mpyr]_{0.50}[FSI]$. In the LMB configuration, this electrode succeeded in providing the actual areal capacity of ≤1.75 mAh/cm² at 0.1C, 50 °C, with a possibility of further improvement through engineering the Li-metal anode and/or separator.

The charge/discharge rate capability of the polymer-binder-free LFP composite cathode with 15 wt% $Li_x[C_2mpyr]_{1-x}[FSI]$ was evaluated to be Li^+-concentration-dependent. Although the polymer-binder-free LFP electrode with 50 mol% Li^+ exhibited a high polarization and performed poorly at higher currents, that with 1 mol% Li^+ showed improved rate performance during both charging and discharging. The 2C/0.1C capacity ratios were 97.2% at 1 mol% Li^+ and 81.4% at 50 mol% Li^+ for lithiation and those were 94.6% at 1 mol% Li^+ and 76.5% at 50 mol% Li^+ for delithiation. Moreover, this LFP cathode with 1 mol% Li^+ had superior capacity and capacity retention. The above Li^+-concentration dependence of battery performance was discussed based on the solubility limit of Li^+ in $Li_x[C_2mpyr]_{1-x}[FSI]$ at the LFP surface.

These findings demonstrate the huge potential of Li^+-containing OIPCs as promising ion-conductive binders to create functional polymer-binder-free electrodes using existing fabrication processes for high-energy-density and high-power-density applications. With the incorporation of Li^+-containing OIPCs in electrodes, their rechargeable batteries not only offer enhanced safety but also can be suitable for a range of applications, to which the current polymer-binder-dependent electrodes cannot be applied. Moreover, the exploration of Li^+-containing OIPCs as ion-conductive binders even opens up the possibility of employing this polymer-binder-free approach in solid-state batteries in the future (*e.g.*, to address the compatibility issue of a conventional binder with a solid electrolyte).

DECLARATIONS

Authors' contributions

D.M.J.: Investigation, Validation, Formal analysis, Data Curation, Writing – Original Draft, Writing – Review & Editing, Visualization. M.F.: Supervision, P.C.H: Supervision, H.U.: Conceptualization, Funding acquisition, Project administration, Supervision, Investigation, Validation, Formal analysis, Data Curation, Visualization, Writing – Original Draft, Writing – Review & Editing.

Availability of data and materials

The data supporting our work can be found in the Supplementary Materials.

Acknowledgments

We would like to thank Mr. Mohand Oumerabet (Bordeaux INP) for his assistance in conducting the electrode stability test (Figure 2g).

Financial support and sponsorship

This project was part of the MESC master program, and this publication acknowledges funding from the European Commission Erasmus+. H.U. acknowledges the Alfred Deakin Postdoctoral Research Fellowship (ADPRF) at Deakin University for support.

Conflicts of interest

All authors declared that there are no conflicts of interest.

Ethical approval and consent to participate

Not applicable.

Consent for publication

Not applicable.

REFERENCES

1. Zubi G, Dufo-López R, Carvalho M, Pasaoglu G. The lithium-ion battery: state of the art and future perspectives. *Renew Sustain Energy Rev* 2018;89:292-308. [DOI: 10.1016/j.rser.2018.03.002]
2. Martins LS, Guimarães LF, Botelho Junior AB, Tenório JAS, Espinosa DCR. Electric car battery: An overview on global demand, recycling and future approaches towards sustainability. *J Environ Manag* 2021;295:113091.[DOI: 10.1016/j.jenvman.2021.113091]
3. Hemavathi S, Srirama S, Prakash AS. Present and future generation of secondary batteries: a review. *ChemBioEng Rev* 2023;10:1123-45. [DOI: 10.1002/cben.202200040]
4. Waseem M, Ahmad M, Parveen A, Suhaib M. Battery technologies and functionality of battery management system for EVs: Current status, key challenges, and future prospectives. *J Power Sources* 2023;580. [DOI: 10.1016/j.jpowsour.2023.233349]
5. Detka K, Górecki K. Selected technologies of electrochemical energy storage—a review. *Energies* 2023;16. [DOI: 10.3390/en16135034]
6. Hannan MA, Hoque MM, Hussain A, Yusof Y, Ker PJ. State-of-the-art and energy management system of lithium-ion batteries in electric vehicle applications: issues and recommendations. *IEEE Access* 2018;6:19362-78. [DOI: 10.1109/access.2018.2817655]
7. Ueda H, Yoshimoto S. Multi-redox active carbons and hydrocarbons: control of their redox properties and potential applications. *Chem Rec* 2021;21:2411-29. [DOI: 10.1002/tcr.202100088]
8. Zu C, Ren Y, Guo F, Yu H, Li H. A reflection on lithium-ion batteries from a lithium-resource perspective. *Adv Energy Sustain Res* 2021;2:2100062. [DOI: 10.1002/aesr.202100062]
9. Manzetti S, Mariasiu F. Electric vehicle battery technologies: From present state to future systems. *Renew Sustain Energy Rev* 2015;51:1004-12. [DOI: 10.1016/j.rser.2015.07.010]

10. Chen J, Liu J, Qi Y, Sun T, Li X. Unveiling the roles of binder in the mechanical integrity of electrodes for lithium-ion batteries. *J Electrochem Soc* 2013;160:A1502-A9. [DOI: 10.1149/2.088309jes]
11. Ram R, Soni V, Khastgir D. Electrical and thermal conductivity of polyvinylidene fluoride (PVDF) – Conducting Carbon Black (CCB) composites: Validation of various theoretical models. *Compos B Eng* 2020;185:107748. [DOI: 10.1016/j.compositesb.2020.107748]
12. Li A, Hempel JL, Balogh MP, Cheng Y-T, Taub AI. Effect of binder content on silicon microparticle anodes for lithium-ion batteries. *J Electrochem Soc* 2023;170:010533. [DOI: 10.1149/1945-7111/acb388]
13. Gordon R, Kassar M, Willenbacher N. Effect of polymeric binders on dispersion of active particles in aqueous LiFePO4-based cathode slurries as well as on mechanical and electrical properties of corresponding dry layers. *ACS Omega* 2020;5:11455-65. [DOI: 10.1021/acsomega.0c00477]
14. Liu G, Zheng H, Song X, Battaglia VS. Particles and polymer binder interaction: a controlling factor in lithium-ion electrode performance. *J Electrochem Soc* 2012;159:A214-A21. [DOI: 10.1149/2.024203jes]
15. Kubarkov AV, Babkin AV, Drozhzhin OA, Stevenson KJ, Antipov EV, Sergeyev VG. Engendering high energy density $LiFePO_4$ electrodes with morphological and compositional tuning. *Nanomaterials* 2023;13. [DOI: 10.3390/nano13111771]
16. Yoon J, Lee J, Kim H, Kim J, Jin H-J. Polymeric binder design for sustainable lithium-ion battery chemistry. *Polymers* 2024;16:254. [DOI: 10.3390/polym16020254]
17. Liang X, Ahmad N, Zhang B, Zeng C, Cao X, Dong Q, Yang W. Research progress of robust binders with superior mechanical properties for high-performance silicon-based lithium-ion batteries. *Mater Chem Front* 2024;8:1480-512. [DOI: 10.1039/d3qm00839h]
18. Qin T, Yang H, Li Q, Yu X, Li H. Design of functional binders for high-specific-energy lithium-ion batteries: from molecular structure to electrode properties. *Ind Chem Mater* 2024;2:191-225. [DOI: 10.1039/d3im00089c]
19. Zhang L, Wu X, Qian W, Pan K, Zhang X, Li L, Jia M, Zhang S. Exploring More Functions in Binders for Lithium Batteries. *Electrochem Energy Rev* 2023;6:198. [DOI: 10.1007/s41918-023-00198-2]
20. Li J, Chen X, Muhammad S, Roy S, Huang H, Yu C, Ullah Z, Wang Z, Zhang Y, Wang K, Guo B. Development of solid polymer electrolytes for solid-state lithium battery applications. *Mater Today Energy* 2024;43:101574. [DOI: 10.1016/j.mtener.2024.101574]
21. Su G, Zhang X, Xiao M, Wang S, Huang S, Han D, Meng Y. Polymeric electrolytes for solid-state lithium ion batteries: structure design, electrochemical properties and cell performances. *ChemSusChem* 2024;17:e202300293. [DOI: 10.1002/cssc.202300293]
22. Meng N, Ye Y, Yang Z, Li H, Lian F. Developing single-ion conductive polymer electrolytes for high-energy-density solid state batteries. *Adv Funct Mater* 2023;33:2305072. [DOI: 10.1002/adfm.202305072]
23. Ueda H, Mizuno F, Kerr R, Forsyth M, Howlett PC. Fast charge and high stability of solid-state graphite organic ionic plastic crystal composite anodes. *Batter Supercaps* 2022;5:e202200057. [DOI: 10.1002/batt.202200057]
24. Hawley WB, Li J. Electrode manufacturing for lithium-ion batteries—Analysis of current and next generation processing. *J Energy Storage* 2019;25:100862. [DOI: 10.1016/j.est.2019.100862]

25. Pringle JM. Recent progress in the development and use of organic ionic plastic crystal electrolytes. *Phys Chem Chem Phys* 2013;15:1339-51. [DOI: 10.1039/c2cp43267f]
26. Zhou Y, Wang X, Zhu H, Armand M, Forsyth M, Greene GW, Pringle JM, Howlett PC. N-ethyl-N-methylpyrrolidinium bis(fluorosulfonyl)imide-electrospun polyvinylidene fluoride composite electrolytes: Characterization and lithium cell studies. *Phys Chem Chem Phys* 2017;19:2225-34. [DOI: 10.1039/c6cp07415d]
27. Wang X, Zhu H, Greene GW, Zhou Y, Yoshizawa-Fujita M, Miyachi Y, Armand M, Forsyth M, Pringle JM, Howlett PC. Organic ionic plastic crystal-based composite electrolyte with surface enhanced ion transport and its use in all-solid-state lithium batteries. *Adv Mater Technol* 2017;2:1700046. [DOI: 10.1002/admt.201700046]
28. Macfarlane DR, Huang J, Forsyth M. Lithium-doped plastic crystal electrolytes exhibiting fast ion conduction for secondary batteries. *Nature* 1999;402:792-4. [DOI: 10.1038/45514]
29. Ueda H. Interphase-driven ion conduction in organic ionic plastic crystal-based solid electrolytes: a review of symmetric cell studies. In: Wandelt K, Bussetti G, editors. Encyclopedia of Solid-Liquid Interfaces. Oxford: Elsevier; 2024.p.743-75.
30. Thomas ML, Hatakeyama-Sato K, Nanbu S, Yoshizawa-Fujita M. Organic ionic plastic crystals: flexible solid electrolytes for lithium secondary batteries. *Energy Adv* 2023;2:748-64. [DOI: 10.1039/d3ya00078h]
31. Wang X, Kerr R, Chen F, Goujon N, Pringle JM, Mecerreyes D, Forsyth M, Howlett PC. Toward High-Energy-Density Lithium Metal Batteries: Opportunities and Challenges for Solid Organic Electrolytes. *Adv Mater* 2020;32:e1905219. [DOI: 10.1002/adma.201905219]
32. Zhu H, MacFarlane DR, Pringle JM, Forsyth M. Organic ionic plastic crystals as solid-state electrolytes. *Trends Chem* 2019;1:126-40. [DOI: 10.1016/j.trechm.2019.01.002]
33. Ueda H, Saito N, Nakanishi A, Zhu H, Kerr R, Mizuno F, Howlett PC, Forsyth M. Unveiling the dynamic change in the ionic conductivity of a solid-state binary mixture comprising an organic ionic plastic crystal and $LiBF_4$. *Mater Today Phys* 2024;43:101395. [DOI: 10.1016/j.mtphys.2024.101395]
34. Forsyth M, Huang J, MacFarlane DR. Lithium doped *N*-methyl-*N*-ethylpyrrolidinium bis(trifluoromethanesulfonyl)amide fast-ion conducting plastic crystals. *J Mater Chem* 2000;10:2259-65. [DOI: 10.1039/b003168m]
35. Henderson WA, Seo DM, Zhou Q, Boyle PD, Shin J-H, De Long HC, Trulove PC, Passerini S. An alternative ionic conductivity mechanism for plastic crystalline salt-lithium salt electrolyte mixtures. *Adv Energy Mater* 2012;2:1343-50. [DOI: 10.1002/aenm.201200130]
36. Nti F, Ueda H, Kang CSM, Greene GW, Pringle JM, Zhu H, Howlett P, Forsyth M, Wang X. Ion transport in Li-Doped Triethyl(methyl)phosphonium tetrafluoroborate (Li-[P_{1222}][BF_4]) impregnated with PVDF nanoparticles. *J Phys Chem C* 2022;126:3839-52. [DOI: 10.1021/acs.jpcc.1c09614]
37. Liang Y, Kerr R, Wang X, Ueda H, Armand M, Forsyth M, Howlett PC. New Plastic Crystal composite electrodes employing delocalized transition metal salts for low-cost, high-safety all-solid-state salt batteries. *Chem Mater* 202410.1021/acs.chemmater.4c01003. [DOI: 10.1021/acs.chemmater.4c01003]
38. Ueda H, Mizuno F, Forsyth M, Howlett PC. Tailoring silicon composite anodes with Li+-containing organic ionic plastic crystals for solid-state batteries. *J Electrochem Soc* 2024;171:020556. [DOI: 10.1149/1945-7111/ad29c5]
39. Del Olmo R, Guzmán-González G, Sanz O, Forsyth M, Casado N. Versatile mixed ionic-electronic conducting binders for high-power, high-energy batteries. *Electrochim Acta* 2024;474:143547. [DOI:

10.1016/j.electacta.2023.143547]

40. Howlett P, Forsyth M, Kerr R, Mendes T, Ueda H, Liang Y, inventors; Deakin University, assignee. Ionic Binders for Solid State Electrodes. WO 2023/019322 A1. 23 Feb 2023.
41. del Olmo R, Mendes TC, Forsyth M, Casado N. Mixed ionic and electronic conducting binders containing PEDOT:PSS and organic ionic plastic crystals toward carbon-free solid-state battery cathodes. *J Mater Chem A* 2022;10:19777-86. [DOI: 10.1039/d1ta09628a]
42. Casado N, Zendegi S, Olmo Rd, Dominguez-Alfaro A, Forsyth M. Tuning electronic and ionic conductivities in composite materials for electrochemical devices. *ACS Appl Polym Mater* 2021;3:1777-84. [DOI: 10.1021/acsapm.0c01315]
43. Li S, Geng Z, Liu L, Wang-Lei D, Su Q, Liao W, inventors; Shanghai Electric Group Co Ltd, assignee. Wide-temperature-range solid electrolyte and application thereof. CN 113140787 A. 20 Jul 2021.
44. Niu H, Wang L, Guan P, Zhang N, Yan C, Ding M, Guo X, Huang T, Hu X. Recent Advances in Application of Ionic Liquids in Electrolyte of Lithium Ion Batteries. *J Energy Storage* 2021;40:102659. [DOI: 10.1016/j.est.2021.102659]
45. Hwang J, Okada H, Haraguchi R, Tawa S, Matsumoto K, Hagiwara R. Ionic liquid electrolyte for room to intermediate temperature operating Li metal batteries: dendrite suppression and improved performance. *J Power Sources* 2020;453:227911. [DOI: 10.1016/j.jpowsour.2020.227911]
46. Gao X, Wu F, Mariani A, Passerini S. Concentrated ionic-liquid-based electrolytes for high-voltage lithium batteries with improved performance at room temperature. *ChemSusChem* 2019;12:4185-93. [DOI: 10.1002/cssc.201901739]
47. Yunis R, Al-Masri D, Hollenkamp AF, Doherty CM, Zhu H, Pringle JM. Plastic crystals utilising small ammonium cations and sulfonylimide anions as electrolytes for lithium batteries. *J Electrochem Soc* 2020;167:070529. [DOI: 10.1149/1945-7111/ab76a2]
48. Yunis R, Newbegin TW, Hollenkamp AF, Pringle JM. Ionic liquids and plastic crystals with a symmetrical pyrrolidinium cation. *Mater Chem Front* 2018;2:1207-14. [DOI: 10.1039/C8QM00016F]
49. Preger Y, Barkholtz HM, Fresquez A, Campbell DL, Juba BW, Romàn-Kustas J, Ferreira SR, Chalamala B. Degradation of Commercial Lithium-Ion Cells as a Function of Chemistry and Cycling Conditions. *J Electrochem Soc* 2020;167:120532. [DOI: 10.1149/1945-7111/abae37]
50. Mao N, Gadkari S, Wang Z, Zhang T, Bai J, Cai Q. A comparative analysis of lithium-ion batteries with different cathodes under overheating and nail penetration conditions. *Energy* 2023;278:128027. [DOI: 10.1016/j.energy.2023.128027]
51. Chen J, Whittingham M. Hydrothermal synthesis of lithium iron phosphate. *Electrochem Commun* 2006;8:855-8. [DOI: 10.1016/j.elecom.2006.03.021]
52. Apachitei G, Hidalgo M, Dogaru D, Lain M, Heymer R, Marco J, Copley M. Optimisation of industrially relevant electrode formulations for lfp cathodes in lithium ion cells. *Batteries* 2023;9:192. [DOI: 10.3390/batteries9040192]
53. Hasa I, Mariyappan S, Saurel D, Adelhelm P, Koposov AY, Masquelier C, Croguennec L, Casas-Cabanas M. Challenges of today for Na-based batteries of the future: From materials to cell metrics. *J Power Sources* 2021;482:228872. [DOI: 10.1016/j.jpowsour.2020.228872]
54. Freiberg A, Metzger M, Haering D, Bretzke S, Puravankara S, Nilges T, Stinner C, Marino C, Gasteiger HA. Anodic decomposition of trimethylboroxine as additive for high voltage li-ion

batteries. *J Electrochem Soc* 2014;161:A2255-A61. [DOI: 10.1149/2.0011501jes]

55. Henderson WA, Young VG, Passerini S, Trulove PC, De Long HC. Plastic phase transitions in *N*-Ethyl-*N*-methylpyrrolidinium Bis(trifluoromethanesulfonyl)imide. *Chem Mater* 2006;18:934-8. [DOI: 10.1021/cm051936f]
56. Zhou Y, Wang X, Zhu H, Yoshizawa-Fujita M, Miyachi Y, Armand M, Forsyth M, Greene GW, Pringle JM, Howlett PC. Solid-state lithium conductors for lithium metal batteries based on electrospun nanofiber/plastic crystal composites. *ChemSusChem* 2017;10:3135-45. [DOI: 10.1002/cssc.201700691]
57. Ramana CV, Mauger A, Gendron F, Julien CM, Zaghib K. Study of the Li-insertion/extraction process in $LiFePO_4/FePO_4$. *J Power Sources* 2009;187:555-64. [DOI: 10.1016/j.jpowsour.2008.11.042]
58. Padhi AK, Nanjundaswamy KS, Goodenough JB. Phospho-olivines as positive-electrode materials for rechargeable lithium batteries. *J Electrochem Soc* 1997;144:1188-94. [DOI: 10.1149/1.1837571]
59. Kim Y, Kim M, Lee T, Kim E, An M, Park J, Cho J, Son Y. Investigation of mass loading of cathode materials for high energy lithium-ion batteries. *Electrochem Commun* 2023;147:107437. [DOI: 10.1016/j.elecom.2023.107437]
60. Deng W, Yin X, Bao W, Zhou X, Hu Z, He B, Qiu B, Meng YS, Liu Z. Quantification of reversible and irreversible lithium in practical lithium-metal batteries. *Nature Energy* 2022;7:1031-41. [DOI: 10.1038/s41560-022-01120-8]
61. Torai S, Nakagomi M, Yoshitake S, Yamaguchi S, Oyama N. State-of-health estimation of $LiFePO_4$/graphite batteries based on a model using differential capacity. *J Power Sources* 2016;306:62-9. [DOI: 10.1016/j.jpowsour.2015.11.070]
62. Homann G, Stolz L, Nair J, Laskovic IC, Winter M, Kasnatscheew J. Poly(Ethylene Oxide)-based electrolyte for solid-state-lithium-batteries with high voltage positive electrodes: evaluating the role of electrolyte oxidation in rapid cell failure. *Sci Rep* 2020;10:4390. [DOI: 10.1038/s41598-020-61373-9]
63. Lee J, Jeong SH, Nam JS, Sagong M, Ahn J, Lim H, Kim ID. Toward thin and stable anodes for practical lithium metal batteries: A review, strategies, and perspectives. *EcoMat* 2023;5:e12416. [DOI: 10.1002/eom2.12416]
64. Cheng H, Tan R, Li J, Huang J, Song W. Coatings on lithium battery separators: a strategy to inhibit lithium dendrites growth. *Molecules* 2023;28:7788. [DOI: 10.3390/molecules28237788]
65. Li Y, Sha L, Lv P, Qiu N, Zhao W, Chen B, Hu P, Zhang G. Influences of Separator Thickness and Surface Coating on Lithium Dendrite Growth: A Phase-Field Study. *Materials* 2022;15:7912. [DOI: 10.3390/ma15227912]
66. Gogia A, Wang Y, Rai AK, Bhattacharya R, Subramanyam G, Kumar J. Binder-Free, Thin-Film Ceramic-Coated Separators for Improved Safety of Lithium-Ion Batteries. *ACS Omega* 2021;6:4204-11. [DOI: 10.1021/acsomega.0c05037]
67. Rafiz K, Murali DRL, Lin JYS. Suppressing lithium dendrite growth on lithium-ion/metal batteries by a tortuously porous γ-alumina separator. *Electrochim Acta* 2022;421:140478. [DOI: 10.1016/j.electacta.2022.140478]
68. Broadhead J, Kuo HC. Electrochemical Principles and Reactions. In: Linden D, Reddy TB, editors. Handbook of Batteries. United States:The McGraw-Hill Companies, Inc.;2002.
69. Gabano JP, Jumel Y, Laurent JF. A Potential–Time Study of the Mass Transfer Phenomena Due to the Lithium Ions in Non-Aqueous Electrolytes. In: Collins DH, editor. Research and Development in

Non-Mechanical Electrical Power Sources;1970.p.255-65.

70. Jin L, Howlett PC, Pringle JM, Janikowski J, Armand M, MacFarlane DR, Forsyth M. An organic ionic plastic crystal electrolyte for rate capability and stability of ambient temperature lithium batteries. *Energy Environ Sci* 2014;7:3352-61. [DOI: 10.1039/c4ee01085j]
71. Sun X-G, Dai S. Electrochemical investigations of ionic liquids with vinylene carbonate for applications in rechargeable lithium ion batteries. *Electrochim Acta* 2010;55:4618-26. [DOI: 10.1016/j.electacta.2010.03.019]
72. Lewandowski A, Świderska-Mocek A. Properties of the graphite-lithium anode in N-methyl-N-propylpiperidinium bis(trifluoromethanesulfonyl)imide as an electrolyte. *J Power Sources* 2007;171:938-43. [DOI: 10.1016/j.jpowsour.2007.06.005]
73. Holzapfel M, Jost C, Prodi-Schwab A, Krumeich F, Würsig A, Buqa H, Novák P. Stabilisation of lithiated graphite in an electrolyte based on ionic liquids: an electrochemical and scanning electron microscopy study. *Carbon* 2005;43:1488-98. [DOI: 10.1016/j.carbon.2005.01.030]
74. Guerfi A, Duchesne S, Kobayashi Y, Vijh A, Zaghib K. $LiFePO_4$ and graphite electrodes with ionic liquids based on bis(fluorosulfonyl)imide $(FSI)^-$ for Li-ion batteries. *J Power Sources* 2008;175:866-73. [DOI: 10.1016/j.jpowsour.2007.09.030]
75. Safari M, Delacourt C. Aging of a Commercial Graphite/$LiFePO_4$ Cell. *J Electrochem Soc* 2011;158:A1123. [DOI: 10.1149/1.3614529]
76. Zhang H, Yang Y, Ren D, Wang L, He X. Graphite as anode materials: Fundamental mechanism, recent progress and advances. *Energy Storage Mater* 2021;36:147-70. [DOI: 10.1016/j.ensm.2020.12.027]
77. Asenbauer J, Eisenmann T, Kuenzel M, Kazzazi A, Chen Z, Bresser D. The success story of graphite as a lithium-ion anode material – fundamentals, remaining challenges, and recent developments including silicon (oxide) composites. *Sustain Energy Fuels* 2020;4:5387-416. [DOI: 10.1039/d0se00175a]
78. Li X, Colclasure AM, Finegan DP, Ren D, Shi Y, Feng X, Cao L, Yang Y, Smith K. Degradation mechanisms of high capacity 18650 cells containing Si-graphite anode and nickel-rich NMC cathode. *Electrochim Acta* 2019;297:1109-20. [DOI: 10.1016/j.electacta.2018.11.194]
79. Abd Elhamid Mahmoud H, Xiao X, Cai MEI, inventors; GM Global Tech Operations LLC, assignee. Multifunction Battery Separator. US 2015/0147641 A1. 28 May 2015.
80. Kim J-H, Pieczonka NPW, Li Z, Wu Y, Harris S, Powell BR. Understanding the capacity fading mechanism in $LiNi_{0.5}Mn_{1.5}O_4$/graphite Li-ion batteries. *Electrochim Acta* 2013;90:556-62. [DOI: 10.1016/j.electacta.2012.12.069]